EDINBURGH INSTRUMENTS

50 YEARS 1971-2021

RMS1000

RAMAN MICROSCOPE

Extending the capabilities to Photoluminescence Microscopy, Time-Resolved Measurements and Fluorescence Lifetime Imaging (FLIM)

- Truly Confocal
- Five-Position Grating Turrets
- Two Spectrograph Options
- Up to Four Simultaneous Detectors

www.edinst.com

Received: 6 May 2021 | Revised: 7 July 2021 | Accepted: 9 July 2021

DOI: 10.1002/jrs.6211

RESEARCH ARTICLE

Journal of RAMAN SPECTROSCOPY WILEY

Association between grade brain tumors and the interleukin-10 receptor subunit alpha based on surface-enhanced Raman spectroscopy and multivariate analysis

Aneta Aniela Kowalska[1] | **Marta Czaplicka**[1] | **Ariadna B. Nowicka**[1] | **Krzysztof Niciński**[1] | **Aleksandra Piotrowska**[2] | **Agnieszka Kamińska**[1]

[1]Institute of Physical Chemistry, Polish Academy of Sciences, Warsaw, Poland

[2]Department of Histology and Embryology, Department of Human Morphology and Embryology, Wroclaw Medical University, Wroclaw, Poland

Correspondence
Aneta Aniela Kowalska and Agnieszka Kamińska, Institute of Physical Chemistry, Polish Academy of Sciences, Kasprzaka 44/52, 01-224 Warsaw, Poland.
Email: akowalska@ichf.edu.pl; akaminska@ichf.edu.pl

Funding information
National Science Centre, Grant/Award Number: 2015/17/B/ST4/04128

Abstract

We present herein a label-free method based on surface-enhanced Raman spectroscopy (SERS) that was performed using a silicon-based SERS platform. The differentiation between primary and secondary brain tumors SERS data was completed partial least squares (PLS) method with a very high 85% of accuracy (in only first and second factors), whereas calculated using principal component analysis (PCA) method gives 74% (in two consecutive components). Additionally, due to the fact that the interleukin-10 (IL-10) cytokine receptor may act in cancer as both an immunosuppressive and an immunostimulant factor, the correlation between the tumor grading and the cytokine receptor are presented. Obtained data indicate that the function of IL-10 cytokine receptor subunit alpha most probably depends or is closely related to the tumor stage.

KEYWORDS

brain tumors, cytokine, interleukin- 10, multivariate analysis, silicon-based SERS platform, surface-enhanced Raman spectroscopy

Highlights

- The correlations between the brain tumor grading and their IL-10 cytokine receptor level are presented.
- Surface-enhanced Raman spectroscopy and the partial least squares regression was applied as methods of differentiations between primary and secondary brain tumors.
- The presented protocol of homogenates tissues analysis may open the way for the new cancer therapy.
- Presented method of tumor differentiation may improve the diagnostic accuracy.

1 | INTRODUCTION

Tumor grading is defined by the World Health Organization (WHO), which incorporates grading and staging and provides a basis for tumor treatments and prognostic prediction.[1] The primary brain tumors, particularly high-grade gliomas, have poor prognosis and patient survival. The secondary tumors (metastases) are spreading from the primary tumor cells to a distant organ via the circulation system. Clinically apparent brain metastases are rare and typically develop in the terminal phases of illness. However, there are statistical evidences that some type of solid tumors, for example, breast cancer in 15%–30% of patients, will develop brain metastases during the course of the disease.[2] Notwithstanding, fewer than 10% of all brain metastases are found before the cancer origin is diagnosed. Nowadays, there is no tool for the differentiation between the primary and secondary brain tumors which can be used just after biopsy or during surgery. As those two cancers are treated differently, it is extremely important to know if a tumor in the brain is a primary or secondary cancer and may prolong the patient life. Thus, to elaborate a technique or even to open the new path for a distinguishing method between those tumors is highly desirable.

It is known that, cytokine network has an important part in cancer and plays a determinant role in the development or regression of different cancers. The level of the cytokines has influences on the production of tumor-inducing or tumor-inhibiting factors, may cause DNA damage, and promote or inhibit angiogenesis. The immunosuppressive cytokine interleukin-10 (IL-10) is still considered as controversial factor.[3] It has been shown that tumor cells, for example, non-small cell lung cancers, melanomas, gliomas, leukemias, and lymphomas, are producing IL-10.[4–7] Therefore, for a long time, this cytokine was considered as a immunostimulating factor controlling the tumor growth; thus, if it is released in response to inflammation, IL-10 inhibits tumor development and progression. However, recently it was shown that IL-10 can work also as an immunosuppressive factor, in other words may support the antitumor function in cancer, and hence the tumor regression, and at the same time, as immunosuppressive factor, may induce tumor invasion and metastasis if it inhibits apoptosis or promote growth.[8] Therefore, broadening the knowledge concerning the level of IL-10 in various tumor cells may significantly increase the survival of oncological patients as the tumor immunotherapy may be adjusted to IL-10 factor. On the other hand, inflammatory IL-10-mediated responses are initiated upon binding to a heterodimeric receptor complex consisting of IL-10 receptors IL-10Rα and IL-10Rβ by molecular recognition paradigm where both of these receptors recognize the same binding site on IL-10. Moreover, a previous study, over the correlation between the expression of IL-10 receptors in CD45+ cells in brain tumor tissues, showed that the CD45+ cell population expressing the IL-10 receptor may have some potential to discriminate between primary tumors and metastases.[9] It was found that the immunophenotype of inflammatory cells differ significantly between tumor types. The studied ratios (CD45+ IL10Rα+/C45+ and CD45+ IL10Rβ+/CD45+) are lower in secondary in comparison with primary tumors. Moreover, as has already been reported, the distinction between healthy and neoplastic cells of brain tumor homogenates can be successfully realized by surface-enhanced Raman spectroscopy (SERS) and principal component analysis (PCA) methods.[10] SERS has already proved that is a powerful technique to study nucleic acids and proteins,[11] therapeutic agents,[12] drugs and trace materials,[13] and microorganisms[14] but also can work as bimolecular sensors for clinical diagnosis of various cancer diseases such as gastrointestinal,[15–17] breast,[18–20] lung,[21,22] and brain cancers.[10,23–26] SERS with a help of PCA[27–31] shows much with higher sensitivity and chemical specificity than that in conventional Raman spectroscopy.[32]

The SERS enhancement factor in the range of 10^4–10^7 depends on the platform configuration and on the type of analyte molecules. Thus, the proper choice of SERS platform may drastically influence the enhancing of signal from the studied molecule. Herein, to amplify the Raman signal of the studied homogenates and further to maximize the spectroscopic differentiation of primary and secondary brain tumors, the silicon-based SERS platform[32] was used. Then, to extend the research on the possibility of using the alpha subunit of IL-10 receptor in brain tumors as a potential differentiating marker; herein, the levels of IL10Rα calculated for samples with known tumor type (primary or secondary) have been correlated with SERS data using both the PCA and the partial least squares regression (PLS) methods.

2 | EXPERIMENTAL SECTION

As part of the presented experimental analysis, eight samples of human brain tissue collected from different people were tested. A total of eight homogenized specimens were analyzed, including two sets of brain tumors, that is, four gliomas (two WHO Grade III and two Grade IV specimens) and four metastatic specimens (Gleason grade: two G2 grade and two G3 grade specimens).

Figure 1 demonstrates the flow of the presented research. Briefly, the human brain tissue samples were treated as follows:

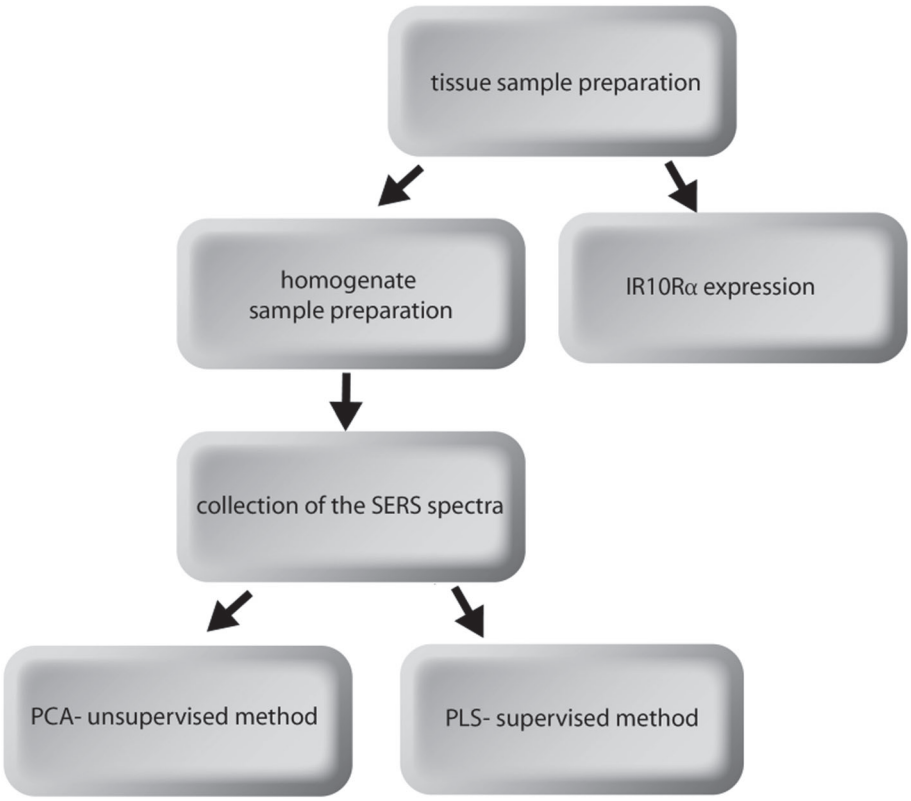

FIGURE 1 The general schematics flow of the presented experiments

a. prepared for both the immunochemistry and SERS experiments via developed homogenate preparation protocol;
b. at the same time, the SERS platforms were fabricated[32] and freshly used in SERS analysis of homogenized tissues;
c. then, using a multivariate approach, the SERS data were analyzed using both the PCA and the PLS methods.

The study was approved by the Bioethical Committee (opinion number 665/2017).

2.1 | Tissue homogenates preparation

It should be mentioned that Raman signals from the biological samples are extremely weak and we are not able to observe any rational spectra even for such long acquisition as 30 min. Therefore, considerable efforts are taken to find the best method for gathering the spectral data of the tumor samples. In this sense, we invented the homogenates preparation,[33,34] which allows to gain satisfactory SERS signal. Tissue fragments were prepared according to an already published procedure. Briefly, tissue fragments were homogenized, first by using low temperature (samples frozen at −80°C). Then samples were enzymatic homogenized using prepared lysis solution (RIPA lysis buffer, 1-mM phenylmethylsulfonic fluoride [PMSF] and inhibitor cocktail [O-Complet Mini: 1 tablet for 10 ml of RIPA buffer]). The solution was incubated in ice for 30 min. Next, the aliquots were homogenized using ultrasonic sonicator (2 min, 180 W) on ice, and then samples were centrifuged at 10.000×*g* for 20 min at 0°C. The supernatant was collected to Eppendorf type tubes and centrifuged again under the above-mentioned conditions. After centrifugation, the supernatant was dropped on freshly prepared SERS platform. The rest of the samples were stored at −20°C for further usages.

2.2 | Immunohistochemistry

Immunohistochemistry reaction was performed on 8-μm slides prepared on cryostat. Slides were air-dried overnight. Initially, endogenous peroxidase was blocked with Envision Flex Peroxidase-Blocking Reagent (Dako) (10 min). Rabbit polyclonal antibody against IL10Rα (MBS2523505, MyBioSource, San Diego, USA) was used as primary antibodies (1:50 in EnVision Flex Antibody Diluent, 20 min.). Then slides were incubated in EnVision FLEX/HRP (20 min). Reaction was visualized with freshly prepared 3,3′-diaminobenzidine (DAB) (5 min). Slides were stained additionally with EnVision Flex Hematoxylin (5 min). After IHC reaction and staining, slides were dehydrated in ethanol (70%, 96%, absolute)

and xylene and then closed with Dako Mounting Medium. IHC reaction was performed on Dako Autostainer Link48. Slides were evaluated under Olympus BX41 light microscope.

2.3 | Preparation SERS platform

Platforms for SERS analysis were prepared based on previously developed silicon-based platform, according to already published procedure.[35] Briefly, the preparation of substrate consists of two stages: cleaning the surface of the silicon panel and applying a layer of SERS-active metal. Briefly, the sample of silicon-based cell with dimensions of about 40 × 40 mm was placed in a petri dish with enough acetone to cover it. In the first step, petri dish with the sample was placed into an orbital shaker and shaken for 15 min with 100 RPM. Then the acetone was poured out and Petri dish was filled with isopropyl alcohol and the shaking stage was repeated. After another 15 min, the stage was repeated for the final time with distilled water (Millipore), still at ambient temperature. The cleaned silicon surface was then dried under the stream of nitrogen and placed in a chamber of physical vapor deposition (PVD) device and sputtered with a 100-nm thick layer of 0.99 % pure silver.

The surface SERS platform characterizations were performed by scanning electron microscopy (SEM) observations under high vacuum using the FEI Nova NanoSEM 450. The accelerating voltage for SEM measurement was ranged from 2 to 10 kV. The SEM images of the prepared SERS platform with homogeneously distributed silver crystals onto a substrate presented on Figure S1 shows the surface in a micrometer scale. The nanostructures that are present on the surface of these larger structures are responsible for plasmon resonance. The median size distribution was determined to be approximately 30 nm with a standard deviation of 10 nm. Based on the AFM analysis,[32] the mean depth of the microstructures was determined to be about 120 nm with a standard deviation of 6 nm.

2.4 | SERS data collection

SERS measurements were performed using the Renishaw inVia Raman system equipped with a 300-mW diode laser emitting a 785-nm line that was used as an excitation source. The laser light was passed through a line filter and focused on a sample mounted on an XYZ translation stage with a 50× objective lens (numerical aperture 0.75) that focused the laser to a spot size of around 2.5 μm. The Raman-scattered light was collected by the same objective through a holographic notch filter to block the Rayleigh scattering. A 1200 groove per millimeter grating was used to provide a spectral resolution of 5 cm^{-1}. The Raman scattering signal was recorded by a 1024 × 256 pixel RenCam CCD detector build up in the Renishaw inVia Raman system. Typically, 30 SERS spectra of the studied samples were acquired for 60 s, with 8 mW of the laser power measured at the sample using mapping mode (3 μm × 3 μm).

2.5 | Multivariate data analysis

The obtained SERS spectra were smoothed with Savitsky–Golay filter; the background was removed using baseline correction (10 itinerary and 64 points), and then the spectra were normalized using a so-called min–max normalization (the area of band around 700 cm^{-1}) using a built-in OPUS software package (Bruker Optic GmbH 2012 version). Then, the PCA was applied (Unscrambler, CAMO software AS, version 10.3, Norway). PCA can be described as uncorrelated linear combination of the original variables (X) as $X = t1p'1 + t2p'2 + \ldots\ 2 + tAp'A + E = TP^{T} + E$, where A is the total number of extracted PCs, t (scores) and p (loadings) are the new latent variables, and E is the residual matrix. Additionally, to further strengthen the analysis, the computed model based on the latent variables in the SERS spectra using supervised pattern classification technique such as the PLS was applied. In the PLS method, the matrix X is decomposed as in the PCA method and a comparable investigation is performed for Y by making a matrix result, U and loads, Q ($Y = UQ^{T} + F$). The objective of PLS is to demonstrate all the constituents forming X and Y so that the residuals for X block, E, and the residuals for Y block, F, are around equal to zero. An inner relationship is additionally built that relates the scores of X block to the scores of Y block.

3 | RESULTS AND DISCUSSION

Two sets of human brain tumors, that is, four gliomas (two WHO Grade III and two Grade IV specimens) and four metastases (Gleason grade: two G2 Grade and two G3 Grade specimens) tumors were collected from different subjects and studied in accordance with the best common practice. The total number of individuals was eight. The homogenization process was performed for each sample, followed by thirty replicates of the SERS spectrum. Tissue sample selection and the preparation protocol and experimental data are described in Section 2.

First, the tumor classification was evaluated using histopathology method and the expression of IL-10Rα was assigned by immunostaining.[9] Analysis of the immunophenotype of cells by flow cytometry is a sensitive and reliable method useful in the assessment of the molecular characteristics of a tumor.[36] The expression levels of IL-10Rα in the control sample are designated as 0. The relative expression levels of the genes in the treated samples are defined as the fold difference compared with the control sample. The experiments were repeated three times. Briefly, to quantify the level of IL-10Rα in the analyzed brain samples, tissues for immunostaining were carefully selected from a series of sections of each brain samples. Nuclear staining with freshly prepared 3,3′-diaminobenzidine (DAB) was performed to differentiate between the individual cells. The number of IL-10Rα cells was counted from images of the 200× magnification under an optical microscope (Figure 2).

The summed and averaged numbers of positive cells from all sections of each tested brain tissues were defined as a value representative of that individual sample. Only cells with staining clearly above background and morphology of taste (spindle) cells and nuclei (based on DAB staining) were counted as positive cells. Moreover, it is worth to notice that the one of innovative aspect of presented method (Figure 1), in relation to those presented on Figure 2 (immunostaining) is the time frame of the entire analysis, i.e. about 1.5 hours for the presented method, while standard histopathology takes usually over 3 weeks. SERS is much faster, spectrum is acquired below 1 minute, and the PCA analysis took few other minutes.

The obtained levels of IL-10Rα in the tissue samples were correlated with the SERS data of the corresponding homogenates. All SERS spectra were acquired in the mapping mode. The repeatability and reproducibility of the received SERS signals of brain tumor homogenates are presented on Figure S2. The relative standard deviation (RSD) estimated for the most intense marker bands at 930 cm^{-1} is about 9%. The presented spectra prove the good reproducibility of collected SERS signal across the platform. Taking into account the characteristic spectral features of the obtained SERS spectra, presented on Figure 3, no substantial differences can be found among presented data for both primary and secondary tumors. This contains important information—on a first view, samples give almost identical spectra independently on tumor grading. Any observed differences among the spectra of each samples, for both primary and secondary samples, are mainly due to the different intensities of the revealed bands. On the other hand, some differences, such as appearance of new bands or shifting, are observed for spectra collected for different tumors belonging to both studied groups. As it was already observed, the band intensities change in the spectra of brain tumors in comparison with the spectra of healthy samples.[10,37,38]

Such spectral variance is explained by different biofunctions of the cells infected by a tumor. Therefore, similar intensity change of the band characteristic for the

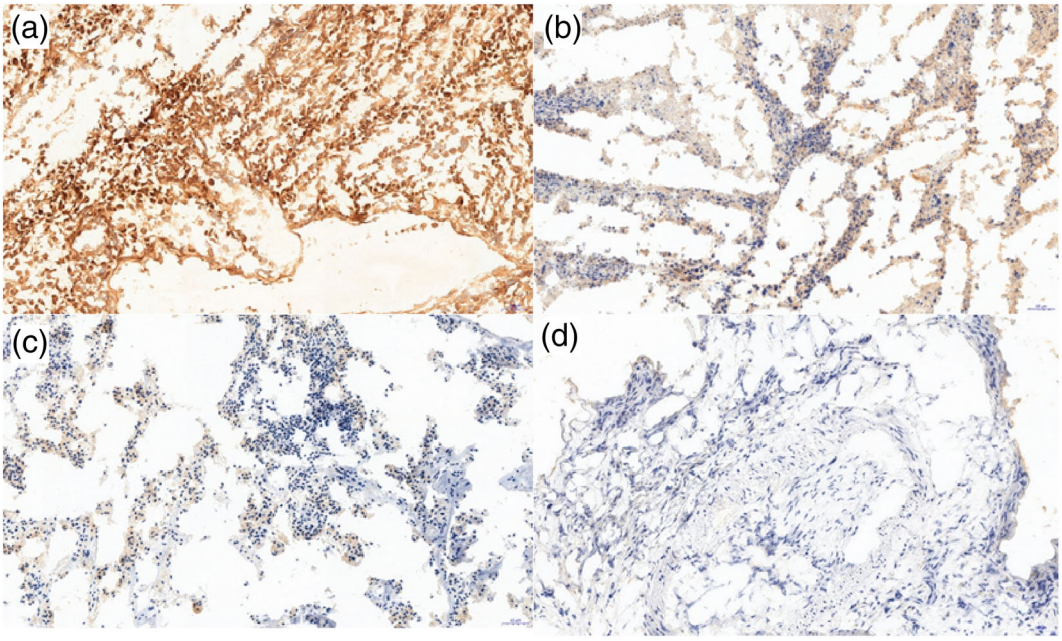

FIGURE 2 Selected histopathological images of IL-10Ra acquired for samples. High (a), moderate (b), low (c) and no expression (d) of IR10Rα. Magnification ×200 [Colour figure can be viewed at wileyonlinelibrary.com]

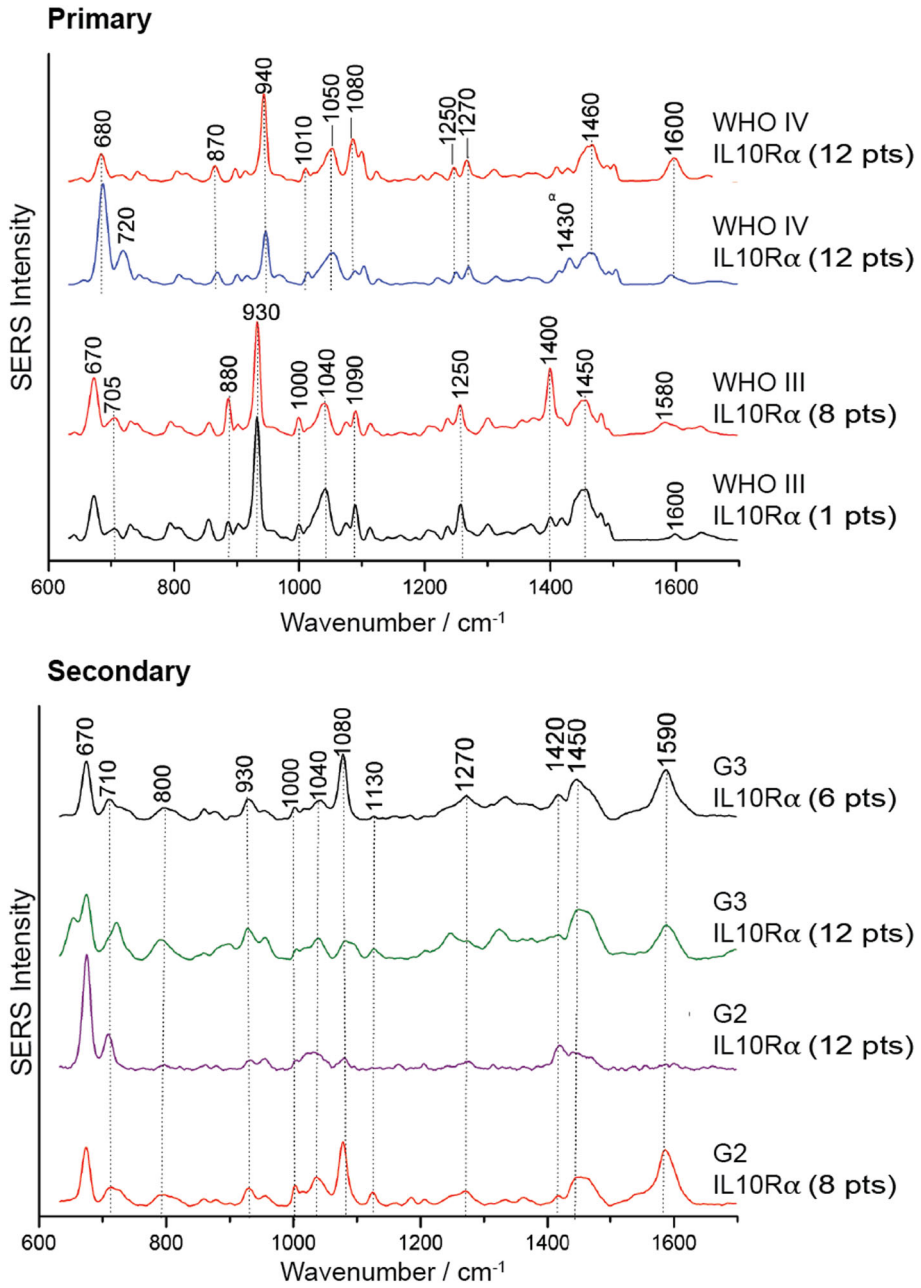

FIGURE 3 Averages SERS spectra of the primary and secondary brain homogenates. Each spectrum is assigned according to WHO classification and IL-10 receptor [Colour figure can be viewed at wileyonlinelibrary.com]

tumor samples is also expected in relation to different tumor stages. As is presented, there are few most intensive bands that can be assigned to L-glutathione and L-histidine vibrations represented by a band at 680/670 cm^{-1}, L-arginine at 870/880 cm^{-1}, guanine at 940/930 cm^{-1}, D-(+)-galactosamine at 1050/1040 cm^{-1}, CC or PO2 symmetric stretching and phospholipids in nucleic acids at 1080/1090 cm^{-1}, L-tryptophan at 1460/1450 cm^{-1}, L-phenylalanine and/or L-alanine at 1580/1590 cm^{-1}, and vibration of the porphyrin moiety of hemoglobin at 1600 cm^{-1}. The assignment of all bands observed in the SERS spectra of the studied samples are gathered in Table S1. All SERS data recorded for both primary and secondary tumor homogenates show little variation in characteristic spectral features. However, the observed differences are not sufficient for discrimination purposes and do not indicate the possibility to use them as indicator for the classification of tumors. Additionally, under each spectrum, the cytokine IL-10Rα receptor for a given sample is shown (Figure 3). There are no specific spectral features that can be directly correlated with this receptor. Thus, to extend this analysis, the multivariate PCA was applied over all recorded SERS data.

The calculated PCA scores are presented on Figure S4. Those analyses were conducted in three sets

of comparisons: (1) primary (WHO III and WHO IV samples), (2) secondary (G2 and G3 grade), and (3) primary and secondary tumors together. Graphically presented plots of the scores of PC1 versus PC2 show good scores distribution among analyzed groups of samples depending from both tumor grading and receptor IL-10Rα level. Figure S4a presents three main groups of scores characteristic for glioma tumors (blue squares WHO III, IL-10Rα [1 pt.], red circles WHO III, IL-10Rα [8 pts], and green triangle for two samples of WHO IV, IL-10Rα [12 pts]) in 2D and 3D version. Taking into account the calculated scores of tumors WHO III grade, they are separated from the scores of tumor IV grade by the PC1 axis. Scores calculated for two groups of WHO IV samples in 2D plots form one group, which is correlated with the same IL-10 receptor (12 pts), whereas on the 3D plots, these scores are divided probably due to difference between individuals, even taking into account age, gender, and so forth. Notably, the scores for WHO IV are located in close proximity to the PC2 axis, but at the same time on the negative side of the PC1 axis, whereas the scores of WHO III samples are on the positive side of the PC1 axis. Additionally, the scores of WHO III are separated by the PC2 axis. These two groups of WHO III grade are characterized with different IL-10R (8 pts and 1 pt) receptors and theirs scores are divided by PC2 axis. All scores calculated for metastases samples presented on 2D figure show scores spreading along the PC1 axis (Figure S4b). However, some tendency can be observed—more scores calculated for G2 samples are on a positive side of the PC1 axis, whereas more scores of G3 samples on its negative side. Moreover, the IL-10Rα (12 pts) revealed for two samples (G2 and G3) are separated from those calculated for two other samples, with smaller IL-10 receptor values, as IL-10R (8 pts) and IL-10R (6 pts) by the PC2 axis. Nevertheless, for all data taken for secondary tumors, presented in 2D figure, there is no obvious border between the scores coming from each groups. Such tendency is rational, as the samples are the same type. Presented on Figure S4c scores calculated for both type, primary and secondary tumors and for primary tumors are separated indicating differences between those samples, which is consistent with their classifications accordingly to WHO. Along the PC1 axis, the difference between the WHO III and IV grade of primary tumors are revealed, whereas along the PC2 axis, the differentiation between primary and secondary tumors can be made. Interestingly, the calculated scores for the three presented comparisons indicate that the first and the second principal components (PC1, PC2) are the most significant and explain the variance of the data as follows: 89% for primary, 68% for secondary, and 74% for both tumors together. The corresponding loadings of PC1 data are presented on Figure S3. Presented loading plots contain features dependent on differences between the studied groups and clearly indicate variables (SERS shifts) responsible for diagnostic segregation over the within-class variance (mostly associated with heterogeneity in tissue sample) of the component. All the most important variables for obtained PC1 as well as the sum of PC1 and PC2 values for all samples are gathered in Table S2.

Additionally, to strengthen the multivariate analysis, the supervised PLS method was applied. In PLS, the projection space of X is explained by both values X and Y. SERS data were divided into a calibration set and a prediction set (automatically chosen spectra; so-called random method). The training set was used to build the model, and calibration set was used to evaluate the obtained model by the root mean square errors of calibration and prediction (RMSEC, RMSEP) and the coefficients of determination of calibration and prediction (R2C, R2P).

The calculated PLS data of three groups (primary, secondary, and primary with secondary tumors together) are presented on Figure 4. Similar to PCA data, Figure S4a shows scores of tumors; both tumors of WHO III grade are separated from the scores of tumor IV grade by the PC1 axis. Moreover, due to the difference in IL-10Rα (8 pts and 1 pt) receptors of WHO III samples, their scores are divided by PC2 axis. This model shows, for F-1 79 % of variance in block Y with 32 % of the spectral data (X matrix), while F-2 explain 9 % of variance in block Y with 32 % of analyzed data. Scores calculated for secondary tumors are presented on Figure 4b. Scores of G2 samples are divided from the scores calculated for G3 samples by the PC1 axis. The PLS model shows, for F-1 34 % of variance in block Y with 28 % of the spectral data (X matrix), while F-2 explain 31 % of variance in block Y with 22 % of data within X matrix. Presented on Figure 4c are scores calculated for primary and secondary tumors. The main PC1 axis divides primary tumors (WHO III from WHO IV), whereas the PC2 axis divides primary from secondary samples. This model explains in F-1 40% with 75% of X and F-2 explains 45%, with 16% of the spectral data (X matrix). Based onto those data calculated, the RMSE and R2 of all three analyzed groups are gathered in Table 1. As an example, the calculated values of the root mean square errors of calibration and prediction (RMSEC = 0.054; RMSEP = 0.056) and the coefficients of determination of calibration and prediction (R2C = 0.981; R2P = 0.980) show good level of the applied model for all, that is, primary and secondary tumor homogenates (Table 1). However, due to the fact that recorded SERS spectra (in applied configuration) are

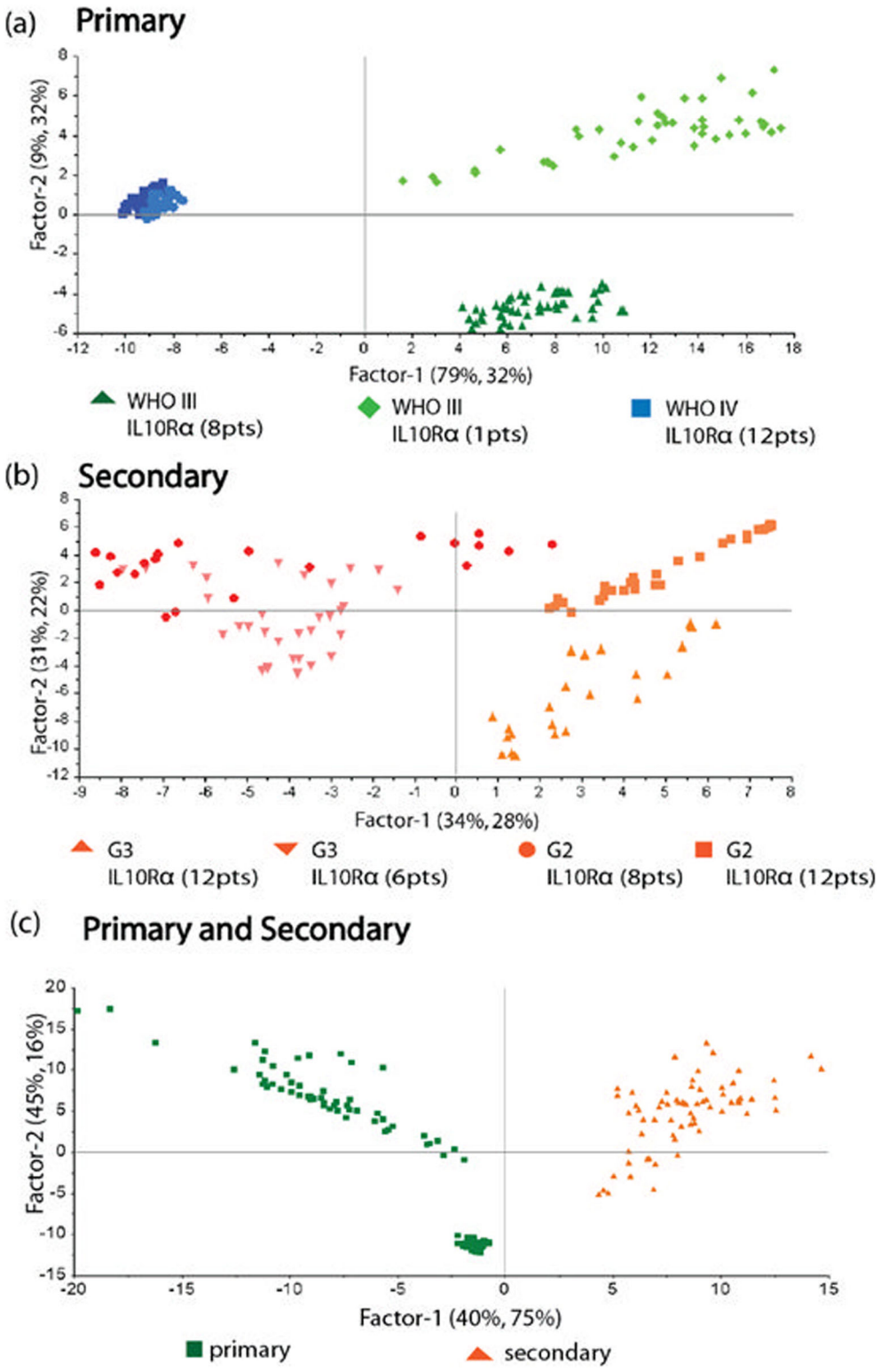

FIGURE 4 The partial least squares regression (PLS) data presented in 2D as the plots of F1 vs. F2 calculated for primary (a), secondary (b), and primary and secondary samples together (c) [Colour figure can be viewed at wileyonlinelibrary.com]

really reproducible across the platform and the Raman signal is strong (see Figure S2), the applied new method of analysis does not substantially expand the obtained correlation.

To summarize, presented studies confirm that the combination of SERS and multivariate analysis allows distinguishing not only homogenates of primary and secondary brain tumors but also individual tumors directly in a given group (according to the WHO classification). At the same time, the method used allows for precise differentiation of the samples in both studied groups due to different levels of IL-10Rα.

TABLE 1 The data obtained from PLS multivariate analysis

PLS	RMSEC	RMSEP	R2C	R2P
Primary and secondary	0.05405	0.05554	0.98120	0.98016
Primary	0.05648	0.05798	0.98512	0.98423
Secondary	0.12098	0.15958	0.92927	0.87119

Abbreviations: PLS, partial least squares regression method; RMSEC, root mean square errors of calibration; RMSEP, root mean square errors of prediction; R2C, coefficients of determination of calibration; R2P, coefficients of determination of prediction.

4 | CONCLUSIONS

The SERS method supported with multivariate analysis enables determining the correlation between the tumor grading and the IL-10Rα level in studied homogenate samples. The presented data revealed that similar to the literature, it is not straightforward to indicate the exact role of IL-10 as immunosuppressive or immunostimulating in a specific sample. However, analyzing the IL-10Rα level with the tumor grade, one can conclude that the probably for the WHO IV samples, IL-10 (IL-10Rα = 12 pts), works rather as an immunosuppressive factor while in the case of WHO III (IL-10Rα = 1p and IL-10Rα = 8p) as an immunostimulating factor. The supervised PLS multivariate method reveals 88%, 65%, and 85% of the variance (using only first and second factors) within the studied data. It should be highlighted that similar analysis cannot be performed using only data based on the standard immunochemistry method.

To summarize, the potential of the proposed method combining SERS with multivariate analysis lies mainly in providing differentiation between the primary and secondary brain tumor homogenates, which may in future applications improve the whole area concerning cancer treatment, diagnostic accuracy, specific cancer diagnosis, risk classification, and development of individual therapeutic strategies.

ACKNOWLEDGMENTS

The authors would especially like to thank Prof. Tomasz Jurek, Dr. L. Szleszkowski, and L. Zadka for sample selection and A. Kmiecik and K. Ratajczak-Wielgomas for clinical sample preparations. The work was supported by National Science Centre, OPUS IX 2015/17/B/ST4/04128.

CONFLICT OF INTEREST

There are no conflicts to declare.

ORCID

Aneta Aniela Kowalska https://orcid.org/0000-0002-1904-9459

REFERENCES

[1] D. N. Louis, A. Perry, G. Reifenberger, A. Von Deimling, D. Figarella, B. Webster, K. C. Hiroko, O. D. Wiestler, P. Kleihues, D. W. Ellison, *Acta Neuropathol.* **2016**, *131*, 803.
[2] E. Tabouret, O. Chinot, P. Metellus, A. Tallet, P. Viens, A. Gonçalves, *Anticancer Res* **2012**, *32*, 4655.
[3] B. C. Asseman, S. Mauze, M. W. Leach, R. L. Coffman, F. Powrie, *J. Exp. Med.* **1999**, *190*, 995.
[4] D. R. Smith, S. L. Kunkel, M. D. Burdick, C. A. Wilke, M. B. Orringer, R. Whyte, R. M. Strieter, *Am. J. Pathol.* **1994**, *145*, 18.
[5] S. Takami, P. McCue, K. Masuoka, S. Salwen, E. C. Lattime, M. J. Mastrangelo, D. Berd, *Clin. Cancer Res.* **1996**, *2*, 1383.
[6] N. Mori, D. Prager, *Leuk. Lymphoma* **1998**, *29*, 239.
[7] N. Voorzanger, R. Touitou, E. Garcia, H.-J. Delecluse, F. Roussert, I. Joab, M. C. Favrot, J.-Y. Blay, *Cancer Res.* **1996**, *56*, 5499.
[8] M. H. Mannino, Z. Zhu, H. Xiao, Q. Bai, M. R. Wakefield, Y. Fang, *Cancer Lett.* **2015**, *367*, 103.
[9] L. Zadka, P. Kram, J. Koscinski, R. Jankowski, M. Kaczmarek, L. Piatek, M. Kulus, A. Gomułkiewicz, A. Piotrowska, P. Dziegiel, *Anticancer Res* **2017**, *37*, 5777.
[10] A. A. Kowalska, S. Berus, Ł. Szleszkowski, A. Kamińska, A. Kmiecik, K. Ratajczak-Wielgomas, T. Jurek, Ł. Zadka, *Spectrochim. Acta - Part a Mol. Biomol. Spectrosc.* **2020**, *231*, 117769. https://doi.org/10.1016/j.saa.2019.117769
[11] K. Kneipp, H. Kneipp, V. B. Kartha, R. Manoharan, G. Deinum, I. Itzkan, R. R. Dasari, M. S. Feld, *Phys. Rev. E* **1998**, *57*, 6281.
[12] R. J. Stokes, E. M. C. Bride, C. G. Wilson, J. M. Girkin, W. E. Smith, D. Graham, *Appl. Spectrosc.* **2008**, *62*, 371.
[13] K. Faulds, W. E. Smith, D. Graham, R. J. Lacey, *Analyst* **2002**, *127*, 282.
[14] A. Sivanesan, E. Witkowska, W. Adamkiewicz, Ł. Drziewit, A. Kamińska, J. Waluk, *Analyst* **2014**, *139*, 1037.
[15] L. M. Almond, J. Hutchings, G. Lloyd, H. Barr, N. Shepherd, J. Day, O. Stevens, S. Sanders, M. Wadley, N. Stone, C. Kendall, *Gastrointest. Endosc.* **2014**, *79*, 37.
[16] C.-W. Hsu, C.-C. Huang, J.-H. Sheu, C.-W. Lin, L.-F. Lin, J.-S. Jin, L.-K. Chau, W. Chen, *PLoS ONE* **2016**, *11*, e0159829.
[17] D. Petersen, P. Naveed, A. Ragheb, D. Niedieker, S. F. El-mashtoly, T. Brechmann, C. Kötting, W. H. Schmiegel, E. Freier, C. Pox, K. Gerwert, *Acta Part a Mol. Biomol. Spectrosc.* **2017**, *181*, 270.
[18] C. J. Frankt, R. L. McCreery, *Anal. Chem.* **1995**, *67*, 777.
[19] A. S. Haka, K. E. Shafer-peltier, M. Fitzmaurice, J. Crowe, R. R. Dasari, M. S. Feld, *Cancer Res.* **2002**, *62*, 5375.

[20] A. S. Haka, K. E. Shafer-peltier, M. Fitzmaurice, J. Crowe, R. R. Dasari, M. S. Feld, *Proc. Natl. Acad. Sci.* **2005**, *102*, 12371.
[21] N. D. Magee, J. S. Villaumie, E. T. Marple, M. Ennis, J. S. Elborn, J. J. Mcgarvey, *J. Phys. Chem. B* **2009**, *22*, 8137.
[22] Z. Huang, A. McWilliams, H. Lui, D. I. McLean, S. Lam, H. Zeng, *Int. J. Cancer* **2003**, *107*, 1047.
[23] C. Krafft, B. Belay, N. Bergner, B. F. M. Romeike, R. Reichart, R. Kalff, J. Popp, *Analyst* **2012**, *137*, 5533.
[24] S. Koljenović, T. C. B. Schut, R. Wolthuis, A. J. P. E. Vincent, G. Hendriks-Hagevi, L. Santos, J. M. Kros, G. J. Puppels, *Anal. Chem.* **2007**, *79*, 557.
[25] S. Koljenovic, L. Choo-smith, T. C. B. Schut, J. M. Kros, H. J. Van Den Berge, G. J. Puppels, *Lab. Invest.* **2002**, *82*, 1265.
[26] K. Gajjar, L. D. Heppenstall, W. Pang, K. M. Ashton, J. Trevisan, I. I. Patel, V. Llabjani, H. F. Stringfellow, P. Martin-Hirsch, T. Dawson, F. L. Martin, *Anal. Methods* **2013**, *44*, 89.
[27] D. Van De Sompel, E. Garai, C. Zavaleta, S. S. Gambhir, *PLoS ONE* **2012**, *7*, e38850.
[28] J. Kiefer, *Analyst* **2015**, *140*, 5012.
[29] A. Matschulat, D. Drescher, J. Kneipp, *ACS Nano* **2010**, *4*, 3259.
[30] B. Kang, S.-S. Li, Q.-Y. Guan, A.-P. Chen, P.-K. Zhang, L.-B. Zhang, J.-W. Wei, J.-J. Xu, H.-Y. Chen, *Chem. Sci.* **2017**, *8*, 1243.
[31] J. Kiefer, K. Noack, *Analyst* **2015**, *140*, 1787.
[32] S. Nie, S. R. Emory, *Science* **1997**, *275*, 1102.
[33] M. Czaplicka, A. A. Kowalska, A. B. Nowicka, D. Kurzydłowski, Z. Gronkiewicz, A. Machulak, W. Kukwa, A. Kamińska, *Anal. Chim. Acta* **2021**, *1177*, 338784.
[34] M. Czaplicka, A. A. Kowalska, A. B. Nowicka, W. Kukwa, Z. Gronkiewicz, D. Kurzydłowski & A. Kamińska. **2020**, Patent Application No. 434777.
[35] K. Niciński, E. Witkowska, D. Korsak, K. Noworyta, J. Trzcińska-Danielewicz, A. Girstun, A. Kamińska, *RSC Adv.* **2019**, *9*, 576.
[36] P. Rhone, B. Ruszkowska-Ciastek, M. Celmer, A. Brkic, K. Bielawski, J. Boinska, E. Zarychta, D. Rosc, *J. Physiol. Pharmacol.* **2017**, *68*, 139.
[37] A. Huang, D. Fuchs, B. Widner, C. Glover, D. C. Henderson, T. G. Allen-mersh, *Br. J. Cancer* **2002**, *86*, 1691.
[38] X. Li, T. Yang, S. Li, D. Wang, Y. Song, S. Zhang, *Laser Phys.* **2016**, *26*, 035702.

SUPPORTING INFORMATION

Additional supporting information may be found online in the Supporting Information section at the end of this article.

How to cite this article: A. A. Kowalska, M. Czaplicka, A. B. Nowicka, K. Niciński, A. Piotrowska, A. Kamińska, *J Raman Spectrosc* **2021**, 1. https://doi.org/10.1002/jrs.6211